



Fermi National Accelerator Laboratory

FERMILAB-Pub-93/169-E

E665

Perturbative QCD Effects Observed in 490 GeV Deep-Inelastic Muon Scattering

The Fermilab E665 Collaboration

*Fermi National Accelerator Laboratory
P.O. Box 500, Batavia, Illinois 60510*

June 1993

Submitted to *Physical Review D*



Disclaimer

This report was prepared as an account of work sponsored by an agency of the United States Government. Neither the United States Government nor any agency thereof, nor any of their employees, makes any warranty, express or implied, or assumes any legal liability or responsibility for the accuracy, completeness, or usefulness of any information, apparatus, product, or process disclosed, or represents that its use would not infringe privately owned rights. Reference herein to any specific commercial product, process, or service by trade name, trademark, manufacturer, or otherwise, does not necessarily constitute or imply its endorsement, recommendation, or favoring by the United States Government or any agency thereof. The views and opinions of authors expressed herein do not necessarily state or reflect those of the United States Government or any agency thereof.

Perturbative QCD Effects Observed in 490 GeV Deep-Inelastic Muon Scattering

THE FERMILAB E665 COLLABORATION

June 7, 1993

Abstract

Results on forward charged hadrons in 490 GeV deep-inelastic muon scattering are presented. The transverse momenta, azimuthal asymmetry, and energy flow of events with four or more forward charged hadrons are studied. The range of the invariant hadronic mass squared $300 < W^2 < 900 \text{ GeV}^2/c^4$ extends higher than previous deep-inelastic muon scattering experiments. Data are compared to the predictions of the Lund Monte Carlo with perturbative QCD simulated by matrix elements, parton showers, and color dipole radiation. Correlations with the multiplicity-independent event variable $\Pi \simeq \sum |p_T|$ are studied. The relationship between the azimuthal asymmetry and transverse momentum of forward hadrons is also presented.

PACS numbers: 13.60Hb, 13.87Ce, 13.87Fh

THE FERMILAB E665 COLLABORATION

M. R. Adams⁶, S. Aïd^{9,a}, P. L. Anthony^{10,b}, M. D. Baker¹⁰, J. Bartlett⁴,
A. A. Bhatti^{13,c}, H. M. Braun¹⁴, W. Busza¹⁰, J. M. Conrad^{5,d}, G. Coutrakon^{4,e},
R. Davisson¹³, I. Derado¹¹, S. K. Dhawan¹⁵, W. Dougherty¹³, T. Dreyer^{1,f},
K. Dziunikowska⁸, V. Eckardt¹¹, U. Ecker^{14,a}, M. Erdmann^{1,g}, A. Eskreys⁷, J. Figiel⁷,
H. J. Gebauer¹¹, D. F. Geesaman², R. Gilman^{2,h}, M. C. Green^{2,i}, J. Haas¹,
C. Halliwell⁶, J. Hanlon⁴, D. Hantke¹¹, V. W. Hughes¹⁵, H. E. Jackson², D. E. Jaffe^{6,j},
G. Jancso¹¹, D. M. Jansen^{13,k}, S. Kaufman², R. D. Kennedy^{3,h}, T. Kirk^{4,l},
H. G. E. Kobrak³, S. Krzywdzinski⁴, S. Kunori⁹, J. J. Lord¹³, H. J. Lubatti¹³,
D. McLeod⁶, S. Magill^{6,m}, P. Malecki⁷, A. Manz¹¹, H. Melanson⁴, D. G. Michael^{5,n},
W. Mohr¹, H. E. Montgomery⁴, J. G. Morfin⁴, R. B. Nickerson^{5,o}, S. O'Day^{9,p},
K. Olkiewicz⁷, L. Osborne¹⁰, V. Papavassiliou^{15,m}, B. Pawlik⁷, F. M. Pipkin^{5,†},
E. J. Ramberg^{9,p}, A. Röser^{14,q}, J. J. Ryan¹⁰, C. W. Salgado⁴, A. Salvarani^{3,r},
H. Schellman¹², M. Schmitt^{5,s}, N. Schmitz¹¹, K. P. Schüller^{15,l}, A. Skuja⁹, G. A. Snow⁹,
S. Söldner-Rembold¹¹, P. H. Steinberg^{9,†}, H. E. Stier^{1,†}, P. Stopa⁷, R. A. Swanson³,
R. Talaga^{9,m}, S. Tentindo-Repond^{2,t}, H.-J. Trost^{2,u}, H. Venkataramania¹⁵,
M. Wilhelm¹, J. Wilkes¹³, Richard Wilson⁵, W. Wittek¹¹, S. A. Wolbers⁴, T. Zhao¹³

¹ Albert-Ludwigs-Universität, D-7800 Freiburg i. Br., Germany

² Argonne National Laboratory, Argonne, Illinois 60439

³ University of California, San Diego, California 92093

⁴ Fermi National Accelerator Laboratory, Batavia, Illinois 60510

⁵ Harvard University, Cambridge, Massachusetts 02138

⁶ University of Illinois, Chicago, Illinois 60680

⁷ Institute for Nuclear Physics, Krakow, Poland

⁸ Institute for Nuclear Physics, Academy of Mining and Metallurgy, Krakow, Poland

⁹ University of Maryland, College Park, Maryland 20742

¹⁰ Massachusetts Institute of Technology, Cambridge, Massachusetts 02139

¹¹ Max-Planck-Institut für Physik, D-8000 Munich-40, Germany

¹² Northwestern University, Evanston, Illinois 60208

¹³ University of Washington, Seattle, Washington 98195

¹⁴ University of Wuppertal, D-5600 Wuppertal, Germany

¹⁵ Yale University, New Haven, Connecticut 06511

† Deceased.

Current addresses:

^a Present address: Büro Schellmann, Rabenhorst 29, Hamburg 65, Germany

^b Present address: Lawrence Livermore National Laboratory, Livermore, California
94550

^c Present address: The Rockefeller University, New York, New York 10021

^d Present address: Columbia University, New York, New York 10027

^e Present address: Loma Linda University Medical Center, Loma Linda, California
92350

^f Present address: RACOS, Maybachstr. 3, D-7750 Konstanz, Germany

^g Present address: DESY, Notkestr. 85, 2000 Hamburg, Germany

^h Present address: Rutgers University, Piscataway, New Jersey 08855

- ⁱ Present address: LeCroy Research Systems, Spring Valley, New York 10977
- ^j Present address: Laboratoire de l'Accélérateur Linéaire, 91405 Orsay, France
- ^k Present address: Los Alamos National Laboratory, Los Alamos, New Mexico 87545
- ^l Present address: SSC Laboratory, Dallas, TX 75237
- ^m Present address: Argonne National Laboratory, Argonne, Il 60439
- ⁿ Present address: California Institute of Technology, Pasadena, California 91125
- ^o Present address: Oxford University, Oxford, OX1 3NP United Kingdom
- ^p Present address: Fermi National Accelerator Laboratory, Batavia, Illinois 60510
- ^q Present address: Ruhruniversität Bochum, D-4630 Bochum 1, Germany
- ^r Present address: A. T. & T, Bell Labs. 2000 North Naperville Road, Naperville, Illinois 60555
- ^s Present address: University of Wisconsin, Madison, Wisconsin 53706
- ^t Present address: Northern Illinois University, Dekalb, Illinois 60115
- ^u Present address: Texas A& M University, College Station, Texas 77843

1 Introduction

In this paper we present measurements, obtained by experiment E665 at Fermilab, of the transverse momenta, energy flow, and azimuthal asymmetry of charged hadrons produced in 490 GeV μp and μd interactions. The data are discussed within the context of the Quark Parton Model and Quantum Chromodynamics. Specific comparisons are made between data and the predictions of the Lund Monte Carlo models. Only hadrons which are forward in the hadronic center-of-mass system are included.

Within the Quark Parton Model, deep-inelastic scattering is described as lepton-parton elastic scattering. The process can be formulated in terms of the one-photon exchange diagram shown in Figure 1a. The momentum of the scattered parton is the vector sum of the intrinsic transverse momentum of the parton and the longitudinal momenta of the incoming parton and virtual photon. The average intrinsic transverse momentum is several hundred MeV/c and thus for large momentum transfers, the scattered parton is very nearly aligned with the photon current direction. The transverse momentum which hadrons acquire in the fragmentation process is also on the average a few hundred MeV/c and is assumed to follow a steeply falling distribution. Thus, in the absence of perturbative QCD effects, forward final state hadrons will be collimated in a narrow jet with respect to the current or virtual photon direction.

The strong interactions between quarks and gluons lead to QCD corrections to the basic scattering picture. The first order in α_S corrections to the one-photon exchange process, gluon bremsstrahlung and photon-gluon fusion, result in two partons, each of which has transverse momentum with respect to the virtual photon

(Figures 1b,c). The subsequent fragmentation of these partons into hadrons can lead to distinguishable hadronic jets [1] which contain particles with high transverse momentum relative to the virtual photon direction. Calculations of the first order QCD corrections show that the average hadronic transverse momentum squared increases with W^2 [2]. We have observed this effect in our data and have compared to previous muon and neutrino deep-inelastic scattering experiments [3]. We will use the term “hard QCD” to refer to the lowest order α_S contributions.

Explicit calculations of the cross-sections for the first-order QCD processes have also shown that the azimuthal distribution (ϕ) of hadrons about the virtual photon direction should be asymmetric with $\langle \cos \phi \rangle$ negative. The azimuthal angle $\phi = 0$ is defined by the projection of the muon scattering plane onto the plane perpendicular to the virtual photon direction (see Figure 2). Gluon bremsstrahlung produces hadrons which prefer to populate the azimuthal range $\pi/2 < \phi < 3\pi/2$ [4, 5]. As was pointed out by Cahn, lowest-order QCD calculations show that the intrinsic transverse momenta of quarks within the nucleon also leads to negative $\langle \cos \phi \rangle$ [6]. In the kinematic range accessible to E665, hard gluon bremsstrahlung and the intrinsic transverse momenta of quarks are both expected to contribute to the azimuthal asymmetry. Recently Chay *et al.*, studying precisely this kinematic range, concluded that the p_T dependence of the azimuthal asymmetry is characteristic of the nature of QCD and the structure of the target hadrons [5]. For hadrons with $p_T > 2 \text{ GeV}/c$ the contribution to $\langle \cos \phi \rangle$ from the intrinsic transverse momentum is small.

The usual Lorentz invariant variables are used in this paper to describe the muon-nucleon scattering process: the energy transferred in the laboratory frame ($\nu = E - E'$) where E and E' are the energies of the incident and scattered muons, respectively; the fraction of the muon laboratory energy transferred ($y_{bj} = \nu/E$); the negative square of the four momentum of the exchanged virtual photon (Q^2); the

Bjorken scaling variable ($x_{bj} = Q^2/2M\nu$); and the virtual photon–nucleon invariant mass squared ($W^2 = M^2 + 2M\nu - Q^2$) where M is the proton mass.

The following variables are used to describe the hadronic system. The transverse momentum, p_T , which is the component of a hadron’s momentum \vec{P}_H perpendicular to the momentum of the virtual photon \vec{q} , where $q^\mu = K_1^\mu - K_2^\mu = (\nu, \vec{q})$. We also use the Feynman variable $x_F \simeq 2p_L^*/W$ which is the scaled longitudinal momentum of a hadron in the virtual photon–nucleon center-of-mass system. When calculating the energy of a hadron E_H , a pion mass is assumed. We further make use of $\Pi \simeq \sum |p_T|$ and planarity variables, discussed in Section 4, first employed by Ballagh *et al.*, which characterize the transverse momentum of an event [7].

2 Description of Experiment

The data presented here come from the sample of μd and μp interactions obtained by E665 during the 1987–88 fixed target run. The E665 open–geometry spectrometer and triggers are discussed in Reference [8]. Here, we restrict ourselves to charged particles detected in the forward spectrometer with $x_F > 0$, which excludes most of the hadrons originating from the target remnant. The trigger used to obtain these data is our Large Angle Trigger (LAT) which requires a muon outside the beam region downstream of the iron hadron absorber. The beam spectrometer determines the incident muon momentum to 0.5%, while the scattered muon momentum is measured in the forward spectrometer to 2.5% at 490 GeV/c. The momentum of charged hadrons is measured in the forward spectrometer to a few percent.

The primary vertex is determined by fitting the incident muon, the scattered muon, and produced hadrons to a common interaction point. Events with reconstructed

multiple muons in the spectrometers were discarded. Events with a reconstructed interaction vertex outside the target were also discarded.

The kinematic cuts applied to the data sample are as follows

$$\begin{aligned}
60 &< \nu < 500 \text{ GeV} \\
Q^2 &> 3.0 \text{ GeV}^2/c^2 \\
0.1 &< y_{bj} < 0.85 \\
100 &< W^2 < 900 \text{ GeV}^2/c^4 \\
x_{bj} &> 0.003
\end{aligned}$$

These cuts include the kinematic regions where the detector has good acceptance, good resolution, and where the backgrounds due to other processes, such as bremsstrahlung or μe scattering, are small.

Figure 3 shows the W^2 distribution for the accepted events after the kinematic and quality cuts described above. E665 nearly doubles the W^2 range that has been accessible to previous deep-inelastic, muon-nucleon scattering experiments.

The events analyzed in this paper were subjected to further selection criteria. Charged hadrons used in these analyses are required to have momentum $P_H > 8 \text{ GeV}/c$, and hadrons which also fit to a secondary vertex are removed. In addition, the distance between the primary vertex and the position of closest approach for hadronic tracks is required to be less than 1.5 cm. The mean distance of closest approach is 1.55 mm for hadrons retained in the event sample. Requirements on track quality, such as χ^2 -probability and the relative error on the hadron momentum ($\Delta P_H/P_H < 5\%$), are also imposed. With these selection criteria, the data sample consisted of approximately 49,000 μ -deuterium and 12,000 μ -hydrogen events. In order to investigate event topologies, a more restrictive W^2 cut, $300 < W^2 < 900$

GeV^2/c^4 and a multiplicity cut are used to select a sub-sample of the data. The selection of events with four or more charged hadrons left 4262 deuterium and 932 hydrogen events. Within statistical errors the data from the two samples are consistent. Further details of this analysis can be found in Reference [9]. The W^2 distribution for this event sample is shown in Figure 4.

To correct for acceptance and radiative effects, we use a Monte Carlo program and Geant 3.12. We use an early version of the Lund program (Lepto 4.3 and Jetset 4.3). This version of Lund, which was initially tuned using European Muon Collaboration (EMC) data, provides a good description of particle distributions and it is adequate for acceptance corrections [10]. The Monte Carlo program simulated the apparatus taking into account chamber efficiencies, secondary interactions, and particle decays. It also takes into account the emission of a photon from either the incident or the scattered muon (radiative corrections) which can alter the event kinematics [11]. These radiative corrections are based on calculations by Mo and Tsai [12]. In general, these corrections increase with p_T^2 and are well-understood. For each bin in an uncorrected distribution, the ratio of reconstructed Monte Carlo and input Monte Carlo has been used as an acceptance factor to correct the data. Correct meson and baryon masses were used as input. All reconstructed charged tracks were assigned pion masses in calculating acceptance corrections. Further details of the Monte Carlo program can be found in Reference [13].

3 Monte Carlo Models

The Monte Carlo models which we use to compare with data after corrections for acceptance and radiative effects have been developed by the Lund group [14, 15]. Perturbative QCD effects are simulated by Lepto 5.2 using matrix elements or parton

Table 1: Lund Monte Carlo models used for physics comparisons.

Interaction	Fragmentation
Matrix Elements, Lepto 5.2	Jetset 6.3
Parton Showers, Lepto 5.2	Jetset 6.3
Color Dipole Radiation, Ariadne 3.0	Jetset 6.3
No Hard QCD, Lepto 5.2	Jetset 6.3

showers. The matrix elements are exact to first order in α_s , whereas the parton shower option, calculated in the leading-log approximation, simulates a part of the higher order effects relevant to the collinear regime. For comparison, Ariadne 3.0 also is used to simulate color dipole radiation in which an emitted gluon, described in terms of the $e^+e^- \rightarrow q\bar{q}g$ matrix element, originates from a color dipole consisting of a quark – antiquark (or diquark) pair [16, 17]. This formalism is different from the Altarelli–Parisi equations which describe gluon radiation as an independent emission from a single parton. The fragmentation process is simulated by Jetset 6.3. The Lund parameters have not been changed from their default values, and no relative normalization has been applied. The Lund distributions shown are as obtained from the generated events, with selection criteria identical to those applied to the data.

The parton distributions used in the Monte Carlo calculation are from Morfin & Tung (fit SL-leading order) [18]. The leading-order fit is the proper choice to use in the Lund Monte Carlo which has matrix elements calculated to leading-order. However, the model predictions presented here are found to be insensitive to the particular choice of parton distribution used.

A summary of the versions of the Lund Monte Carlo to which we compare the data is presented in Table 1. The no-hard-QCD predictions are obtained by “turning off” the QCD matrix elements in Lepto 5.2.

4 Results

The underlying partonic substructure of a hard QCD event naturally defines an event plane which contains the virtual photon and the $q\bar{q}$ or gg pair. In this plane, the net hadronic transverse momentum squared (relative to the virtual photon direction) is maximal. Empirically, we approximate the event plane with the plane defined by the virtual photon three-momentum, \vec{q} , and the vector \vec{N}_1 (perpendicular to \vec{q}) which is determined by maximizing

$$\sum p_{T,in}^2 = \sum (\vec{P}_H \cdot \hat{N}_1)^2 \quad (1)$$

The quantity $p_{T,in}$ is the component of the hadron's transverse momentum lying in the hadronic event plane and the sum is over all hadrons in the event which meet the acceptance criteria.

Every hadron has a $p_{T,in}$ which lies in the event plane and a $p_{T,out}$ which is perpendicular to the event plane. Normalized $\sum p_{T,in}^2$ and $\sum p_{T,out}^2$ distributions are shown in Figures 5a,b along with predictions of the Lund Monte Carlo models. As expected from hard QCD, the $\sum p_{T,in}^2$ distribution is considerably broader than the $\sum p_{T,out}^2$ distribution. The Lund model predictions with hard QCD included are consistent within the statistical significance of the data.

Gluon bremsstrahlung and photon-gluon fusion events will have, on average, larger values of transverse energy E_T (or $\sum |p_T|$) and $\sum |p_{T,in}| > \sum |p_{T,out}|$. Therefore we use the combination of two event variables, first introduced by Ballagh *et al.* [7], to select events expected to contain an increased fraction of hard QCD events:

$$\Pi = \frac{4}{\sqrt{n_H}} \sum (|p_T| - p_{T^0}) \quad (2)$$

$$\underline{P} = \frac{\sum (p_{T,in}^2 - p_{T,out}^2)}{\sum (p_{T,in}^2 + p_{T,out}^2)} \quad (3)$$

The variable Π is an extension of the variable $\Pi_T \cong \sum_{partons} |p_T|$ introduced by Georgi and Sheiman [19]. The constant $p_{T^0} = 0.32$ GeV/c used by Ballagh *et al.*, moves the most probable value of the distribution to zero and the square-root of the number of charged hadrons, $\sqrt{n_H}$, reduces the dependence of the distribution on multiplicity. The planarity, \underline{P} , is a measure of the transverse shape of the event. The quantities Π and \underline{P} have also been used in an analysis of data from a BEBC neutrino-nucleon scattering experiment [20].

Figure 6 shows the normalized Π distribution for events with $W^2 > 300$ GeV²/c⁴. Predictions of the Monte Carlo models are also shown. The Monte Carlo models with hard QCD give a good description of the data whereas the model without hard QCD processes fails to reproduce the observed number of high Π events. From Figure 6 it is apparent that selecting events with large values of Π ($\Pi > 3.0$) should significantly enhance the fraction of hard QCD events.

The scatter plot of Π versus planarity for events with $W^2 > 300$ GeV²/c⁴ is shown in Figure 7a. The data show that events with large Π also have a planar topology. The Lund Monte Carlo prediction with no hard QCD, shown in Figure 7b, has very few events with $\Pi > 3.0$ and no correlation between Π and \underline{P} . The Lund Monte Carlo supports the interpretation that the events selected by $\Pi > 3.0$ and $\underline{P} > 0.5$ originate from hard QCD processes. The scatter plots shown in Figures 7a,b both contain the same number of entries.

In Figure 8 we show the predictions of the Lund Monte Carlo (matrix-elements option) for the Π dependence of the relative contribution of quark scattering, gluon bremsstrahlung, and photon-gluon fusion. In addition to the general selection criteria, the requirements $\underline{P} > 0.5$ and $W^2 > 300$ GeV²/c⁴ are imposed. The fraction of event types for $\Pi > 2.5$ is not very sensitive to the invariant mass (m_{ij}) threshold of

the parton pair used in the Lund Monte Carlo or the choice of parton distribution functions (see Reference [9]).

The data shown in Figure 8 for the fraction of events remaining in the event sample as one increases the Π cut are in good agreement with the Lund Monte Carlo prediction. The Monte Carlo calculation indicates that for $\Pi > 3.0$, approximately 55% of the events are due to photon-gluon fusion and 40% of the events are due to gluon bremsstrahlung.

The normalized p_T^2 distribution (average multiplicity per unit p_T^2) for events with $W^2 > 300 \text{ GeV}^2/c^4$ is shown in Figure 9a. There are a significant number of entries at large p_T^2 which are consistent with the Lund hard QCD prediction. We note that the Lund Monte Carlo with no hard QCD has a considerably softer p_T^2 distribution as expected. Figure 9b shows the effect of imposing the $\Pi > 3.0$ and $\underline{P} > 0.5$ cuts. Again the agreement with the Lund hard QCD prediction is good. The complementary cut $\Pi < 3.0$ or $\underline{P} < 0.5$ has a softer distribution and is also well reproduced by the Lund prediction. The three QCD Lund Monte Carlo models, summarized in Table 1, all give a good description of the data.

The scaled angular energy flow, projected onto the event plane, is defined as

$$\frac{d \langle E/W \rangle}{d\psi} = \frac{1}{N_{ev} \Delta\psi} \sum_{i=1}^{N_{ev}} \sum_{j=1}^{N_h} \frac{E_j^*}{W_i} \quad (4)$$

in the virtual photon-nucleon center-of-mass system, where N_h is the number of hadrons in the i th event which are in the interval $\Delta\psi$ and N_{ev} is the number of events surviving cuts. The double sum is over all hadrons contained in the accepted events and in these distributions $\psi < 0$ is specified by the projection of the muon onto the event plane. The angle ψ^j is defined by $\psi^j \equiv \arctan(p_{T,in}^j/p_L^{*,j})$ where $p_L^{*,j}$ is the longitudinal momentum of the j th hadron (see Figure 10). Figure 11 shows the angular energy flow for events with $W^2 > 300 \text{ GeV}^2/c^4$, $\underline{P} > 0.5$ and two Π

cuts. The angular energy flow for the events with $\Pi > 3.0$ shows two well separated lobes in quantitative agreement with the QCD based Lund predictions. Events with $\Pi > -1.0$, which have a large percentage of low p_T values, show a single jet structure consistent with the Lund model predictions. We note that the acceptance for the range $-45^\circ < \psi < 45^\circ$ is approximately constant [9]. We have also verified that the selection $\Pi > 3.0$ does not artificially introduce a minimum at $\psi = 0$ in Monte Carlo events with no hard QCD [9].

The results presented thus far are consistent with expected hard QCD effects. We now turn to azimuthal distributions of hadrons about the virtual photon direction; as discussed in the Introduction, asymmetries in these distributions can be attributed to gluon bremsstrahlung and the intrinsic transverse momenta of quarks.

Figure 12 shows the normalized ϕ distributions of hadrons about the virtual photon direction for events with $\Pi < 1.0$ and $\Pi > 1.0$. In addition, we impose $W^2 > 300 \text{ GeV}^2/c^4$ and require hadrons to have $x_F > 0.2$ ($x_F > 0.2$ ensures good track acceptance). The $\Pi < 1.0$ distribution is consistent with little or no asymmetry. A good fit, $\chi^2/\text{df} = 0.59$ can be obtained for an isotropic distribution $1/N_{ev} dN_H/d\phi = A$. The curves shown are fits to

$$\frac{1}{N_{ev}} \frac{dN_H}{d\phi} = A + B \cos \phi + C \cos 2\phi + D \sin \phi \quad (5)$$

For events with $\Pi > 1.0$, the hadrons prefer to be opposite the projection of the muon which is at $\phi = 0$. Energy weighted distributions show a similar asymmetry.

Figures 13 and 14 show the average value of $\cos \phi$ as a function of the transverse momentum cutoff P_{TC} .¹ In contrast to Figure 12, in these figures we take events with one or more forward charged hadrons but retain the $300 < W^2 < 900 \text{ GeV}^2/c^4$ cut. All other selection criteria are identical to those described in Section 2. Hadrons with

¹Similar plots presented in References [5, 9] were not corrected for acceptance.

transverse momentum greater or equal to the cut value, specified by the horizontal axis, are retained in the data sample. Data are compared to the theoretical model developed by Chay *et al.* which includes both perturbative and nonperturbative effects [5]. In this model, both the intrinsic transverse momentum (k_T) and the fragmentation transverse momentum (p_F) are assumed to be Gaussian distributed. Figures 13 and 14 show the effect of varying $\langle k_T \rangle$ and $\langle p_F \rangle$, respectively. The model with $\langle k_T \rangle = 0.5$ GeV/c and $\langle p_F \rangle = 0.7$ GeV/c is consistent with the data.

The angular asymmetry is sensitive to both the intrinsic and fragmentation transverse momenta distributions for $P_{TC} < 2.0$ GeV/c. Chay *et al.* point out that in this range we are dominated by non-perturbative effects [5]. From the curves shown in Figures 13 and 14 it is seen that as one increases the transverse momentum cutoff above ≈ 1.5 GeV/c, the expected contribution from intrinsic transverse momentum decreases. A further point made by Chay *et al.* is that photon-gluon fusion events will not exhibit $\cos \phi$ asymmetry if one sums all forward hadrons. The small size of our statistical sample requires such a summation. Since these data are predominantly at low x_{bj} , ($\langle x_{bj} \rangle = 0.038$), we do have significant contributions from photon-gluon fusion and the summation over z further dilutes the hard QCD asymmetry due to gluon bremsstrahlung. We conclude that the observed ϕ asymmetry arises from the intrinsic transverse momentum of the partons, a conclusion consistent with an earlier analysis at lower W^2 by the European Muon Collaboration [21].

5 Summary

Charged hadrons produced in deep-inelastic muon scattering have been studied. Event variables Π and \underline{P} , based on the transverse momentum properties of hadrons, have been used to study events with different topologies. Events with $\Pi > 3.0$ and $\underline{P} > 0.5$ have a two-lobe structure, and by definition contain high transverse momentum hadrons and a planar topology. These characteristics are expected for events originating from first order perturbative QCD processes, gluon bremsstrahlung and photon-gluon fusion. The QCD based Monte Carlo models developed by Lund give good quantitative agreement with the data. Event with large Π show significantly enhanced $\cos \phi$ asymmetries compared to events with $\Pi \sim 0$. However, on further analysis we find that most of the observed asymmetry arises from intrinsic transverse momentum consistent with the conclusions of the EMC analysis.

We wish to thank all those personnel, both at Fermilab and the participating institutions, who have contributed to the success of this experiment. We also thank S. Ellis for illuminating discussions. The work of the University of California, San Diego was supported in part by the National Science Foundation, contract numbers PHY82-05900, PHY85-11584 and PHY88-10221; the University of Illinois at Chicago by NSF contract PHY88-11164; and the University of Washington by NSF contract numbers PHY83-13347 and PHY86-13003. The University of Washington was also supported by the U. S. Department of Energy. The work of Argonne National Laboratory was supported by the Department of Energy, Nuclear Physics Division, under Contract No. W-31-109-ENG-38. The Department of Energy, High Energy Physics Division, supported the work of Harvard University, the University of Maryland, the Massachusetts Institute of Technology under Contract No. DE-AC02-76ER03069, Northwestern University and Yale University. University. The

Albert-Ludwigs-Universität and the University of Wuppertal were supported in part by the Bundesministerium für Forschung und Technologie.

References

- [1] M.R. Adams *et al.*, Phys. Rev. Lett. **69**, 1026 (1992).
- [2] G. Altarelli and G. Martinelli, Phys. Lett. B **76**, 89 (1978).
- [3] M.R. Adams *et al.*, Phys. Lett. B **272**, 163 (1991).
- [4] H. Georgi and H. D. Politzer, Phys. Rev. Lett. **40**, 3 (1978).
- [5] J. Chay, S.D. Ellis, and J.W. Stirling, Phys. Rev. D **45**, 46 (1992), and Phys. Lett. B **269**, 175 (1991).
- [6] R.N. Cahn, Phys. Lett. B **78**, 269 (1978).
- [7] H.C. Ballagh *et al.*, Phys. Rev. Lett. **47**, 556 (1981).
- [8] M.R. Adams *et al.*, Nucl. Instr. Meth. **291**, 533 (1990).
- [9] D. M. Jansen, “Transverse Momentum and the Energy Flow of Charged Hadrons Produced in 490 GeV/c Deep Inelastic Muon Scattering”, University of Washington, Ph.D. thesis (1991)
- [10] T. Sjöstrand, Comput. Physics Commun. **27**, 243 (1982).
- [11] J. Drees, “Radiative Corrections and Hadron Distributions in Deep Inelastic Muon Proton Scattering”, Department of Physics, University of Wuppertal, WU - B, 78 -16 (1978)
- [12] L.W. Mo and Y.S. Tsai, Rev. Mod. Phys. **41**, 205 (1969).
- [13] S. Kunori and S. Aïd, E665 Internal Note MC012, “E665 Monte Carlo Program”; S. Wolbers, E665 Internal Note MC010, “The E665 Second Stage Monte Carlo Program”. See also Reference [9].

- [14] G. Ingelman, “The Lund Monte Carlo for Lepton – Nucleon Scattering, Lepto Version 5.2”, program manual, 1987; M. Bengtsson *et al.*, Nucl. Phys. B **301**, 554 (1988).
- [15] M. Bengtsson and T. Sjöstrand, “Parton Showers in Leptoproduction Events”, University of Lund, LU TP 87–10 (1987).
- [16] L. Lönnblad and U. Pettersson, “Ariadne 3.0 : A Monte Carlo Program for Colour Dipole Radiation”, program manual, 1989.
- [17] B. Andersson *et al.*, Z. Phys. C **43**, 625 (1989).
- [18] J. Morfin and Wu-ki Tung, Z. Phys. C **52**, 13 (1991).
- [19] H. Georgi and J. Sheiman, Phys. Rev. D **20**, 111 (1979).
- [20] P.C. Bosetti *et al.*, Z Phys. C **46**, 377 (1990).
- [21] M. Arneodo *et al.*, Z Phys. C **34**, 277 (1987)

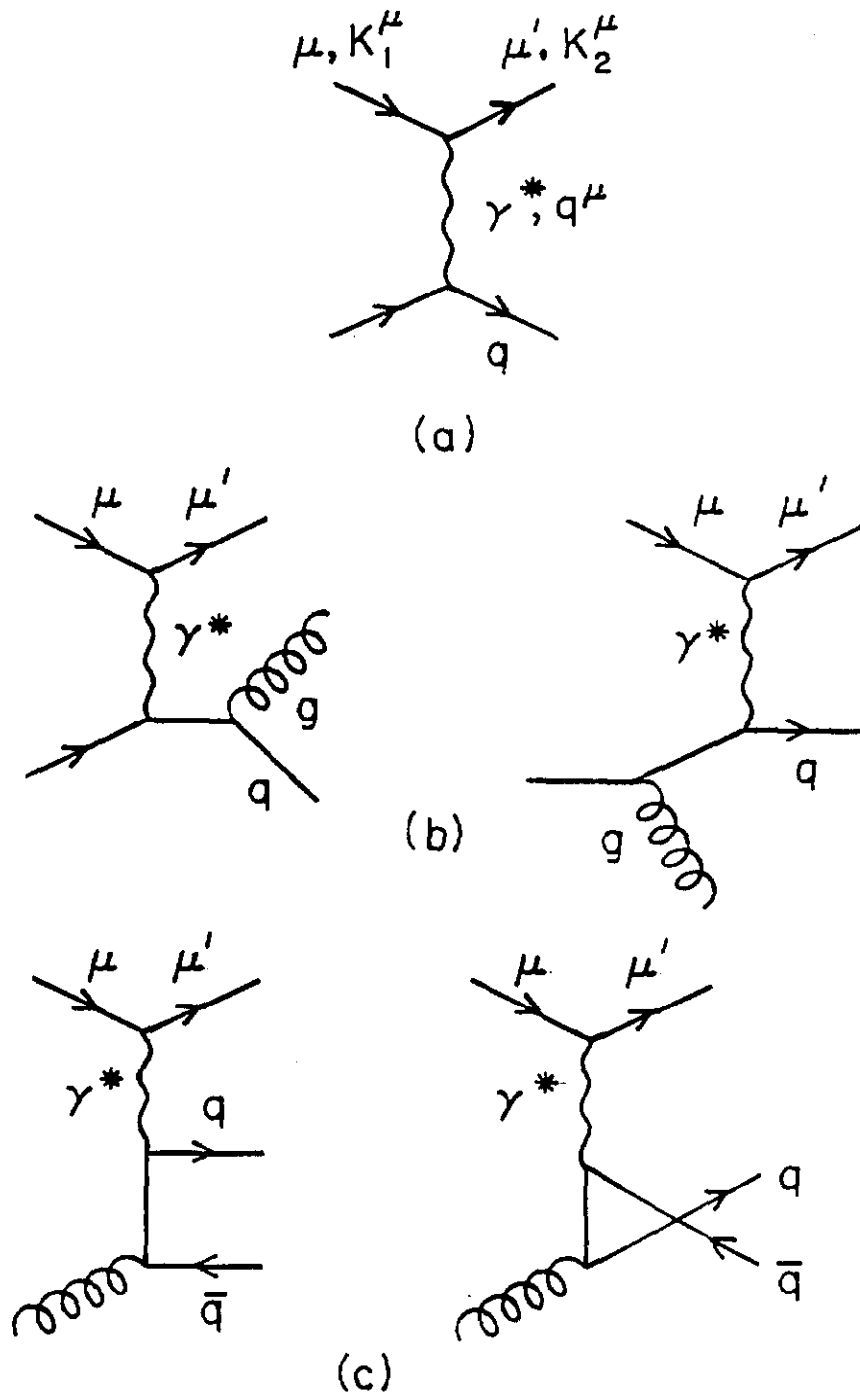


Figure 1: Deep inelastic muon scattering, a: quark scattering, b: gluon bremsstrahlung, c: photon-gluon fusion.

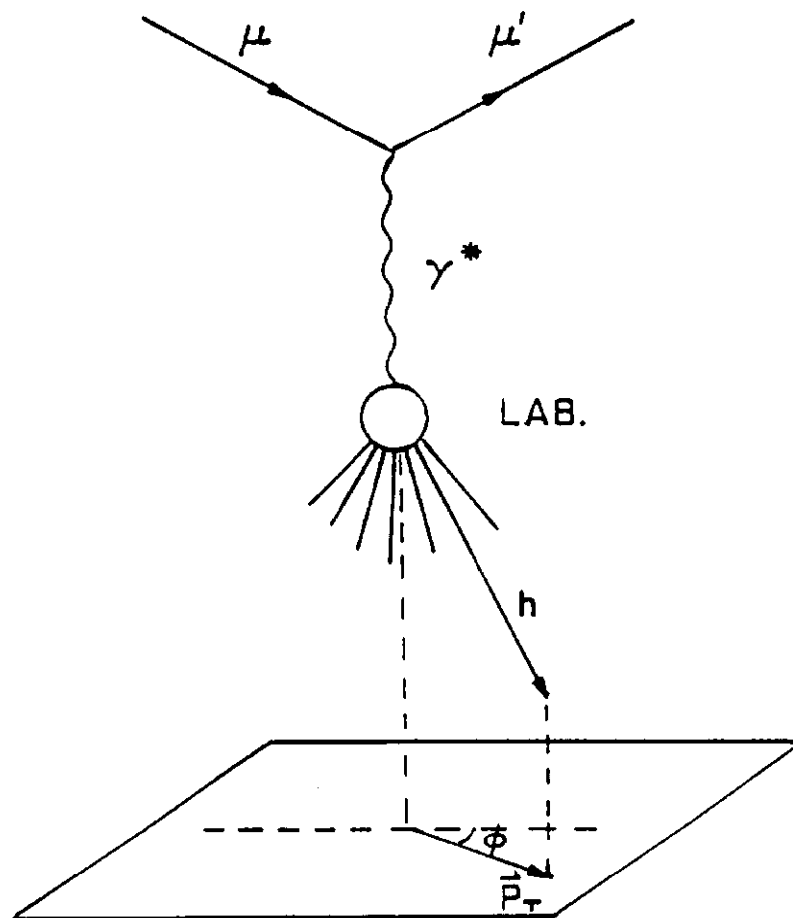


Figure 2: Definition of azimuthal angles for produced hadrons (see text).

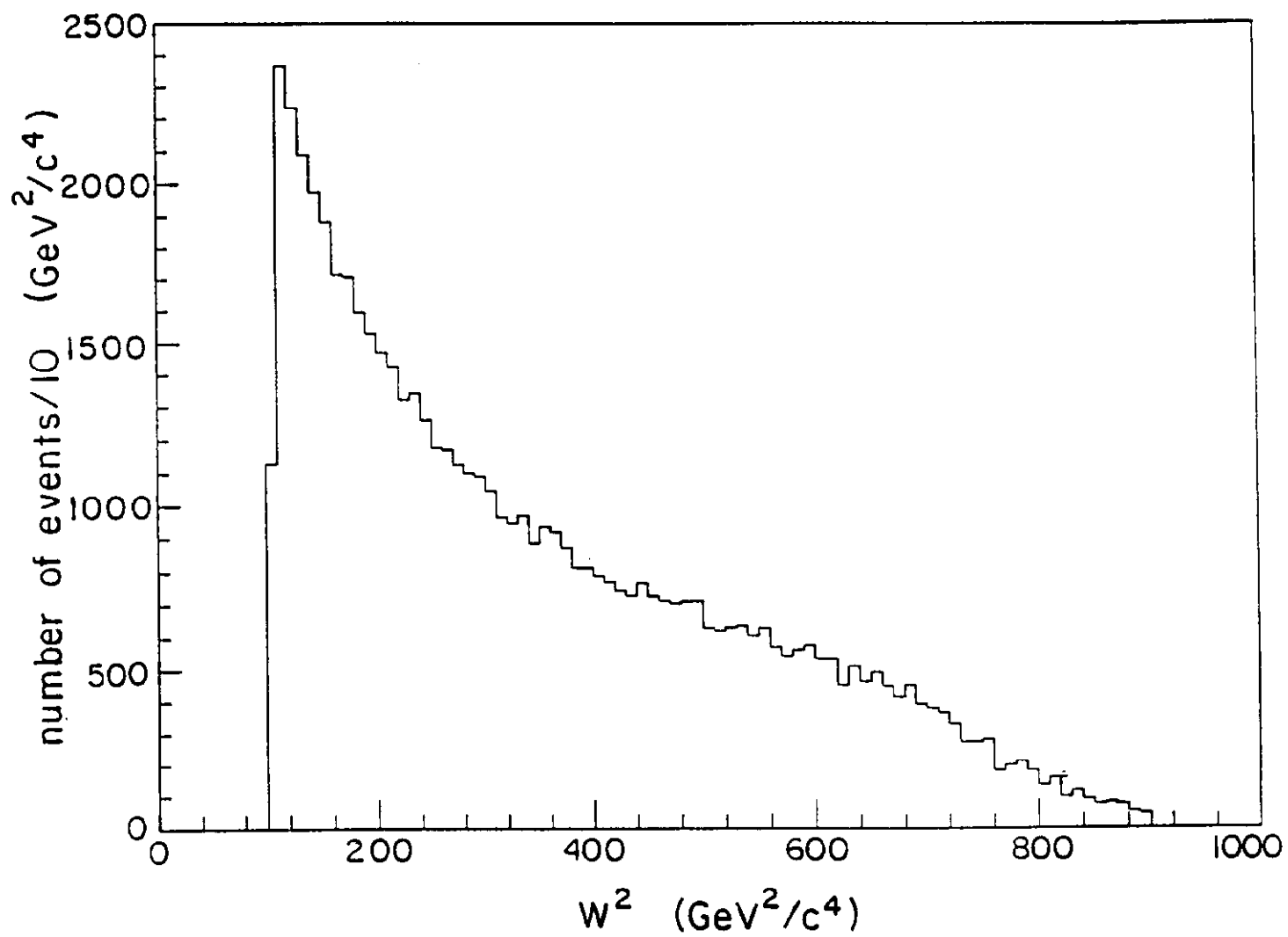


Figure 3: The uncorrected W^2 distribution for the data sample after the kinematic cuts but before multiplicity cuts.

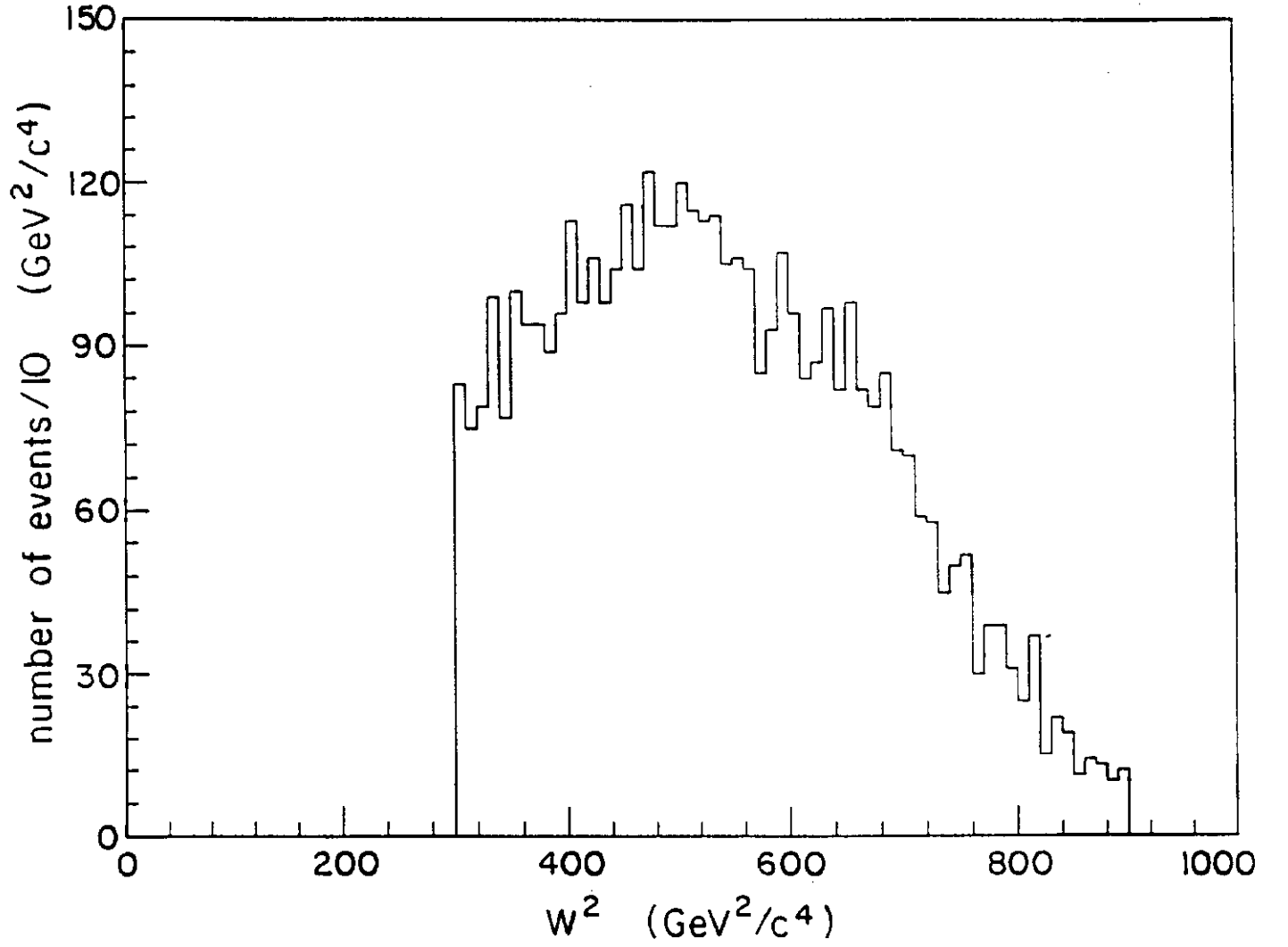


Figure 4: The uncorrected W^2 distribution for the data sample used in this paper, after the $300 < W^2 < 900 \text{ GeV}^2/c^4$ and $n_{ch} \geq 4$ cuts.

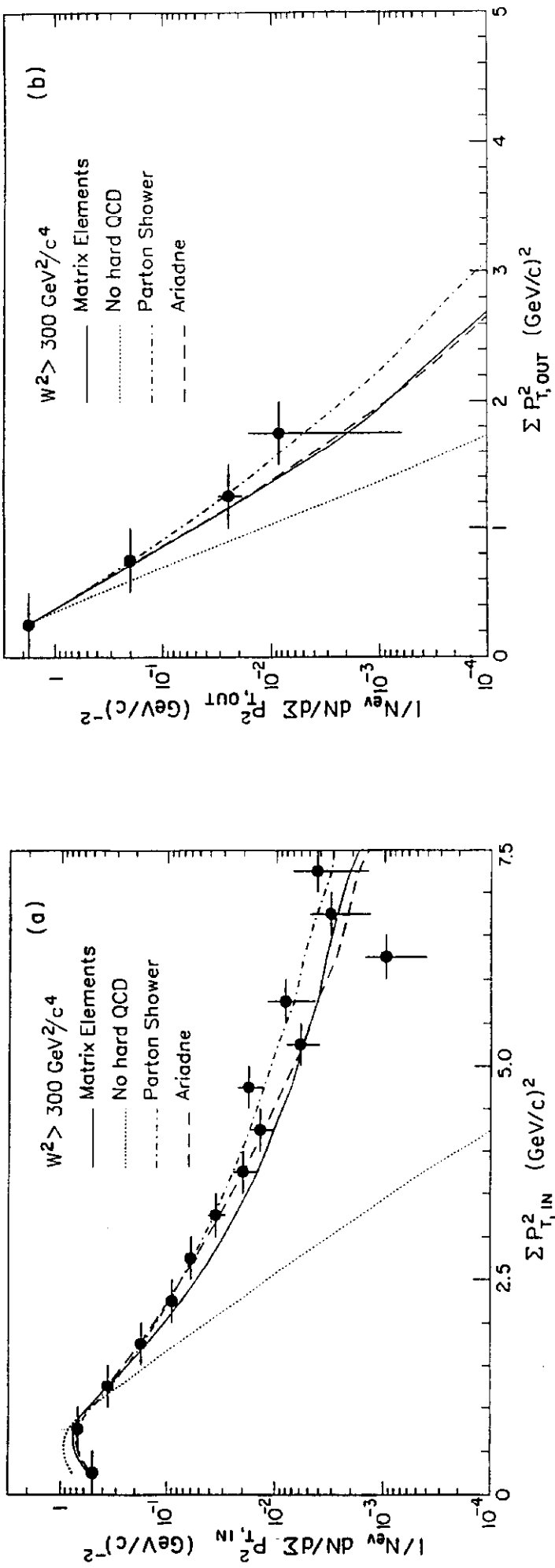


Figure 5: Normalized a: $\Sigma p_{T,\text{in}}^2$ and b: $\Sigma p_{T,\text{out}}^2$ distributions for events with $W^2 > 300 \text{ GeV}^2/c^4$ and ≥ 4 charged hadrons. The data are corrected for acceptance. The curves are various LUND Monte Carlo calculations described in the text.

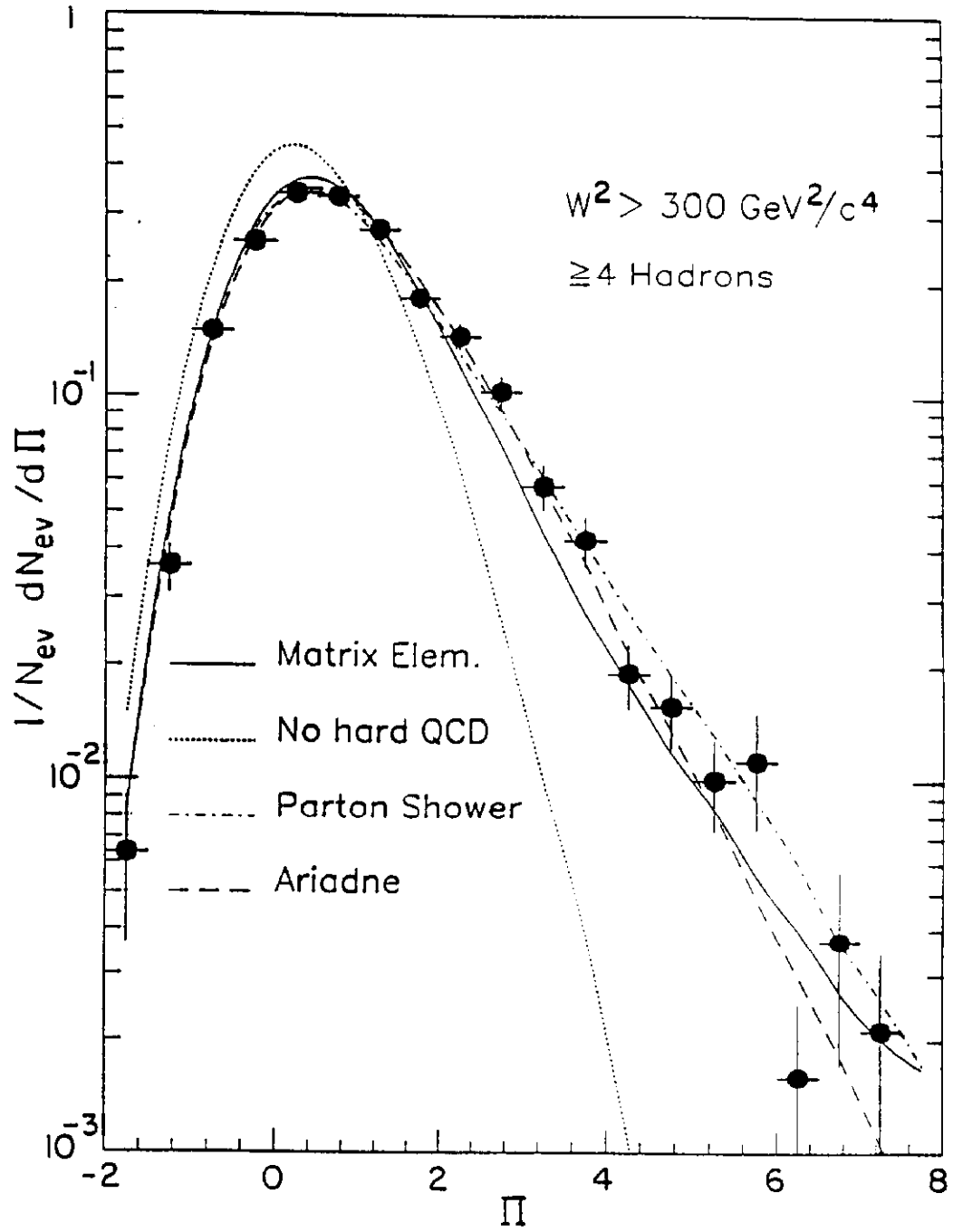


Figure 6: Normalized Π distribution for events with $W^2 > 300 \text{ GeV}^2/c^4$ and ≥ 4 charged hadrons. Data, which are corrected for acceptance, are compared to predictions of the Lund Monte Carlo.

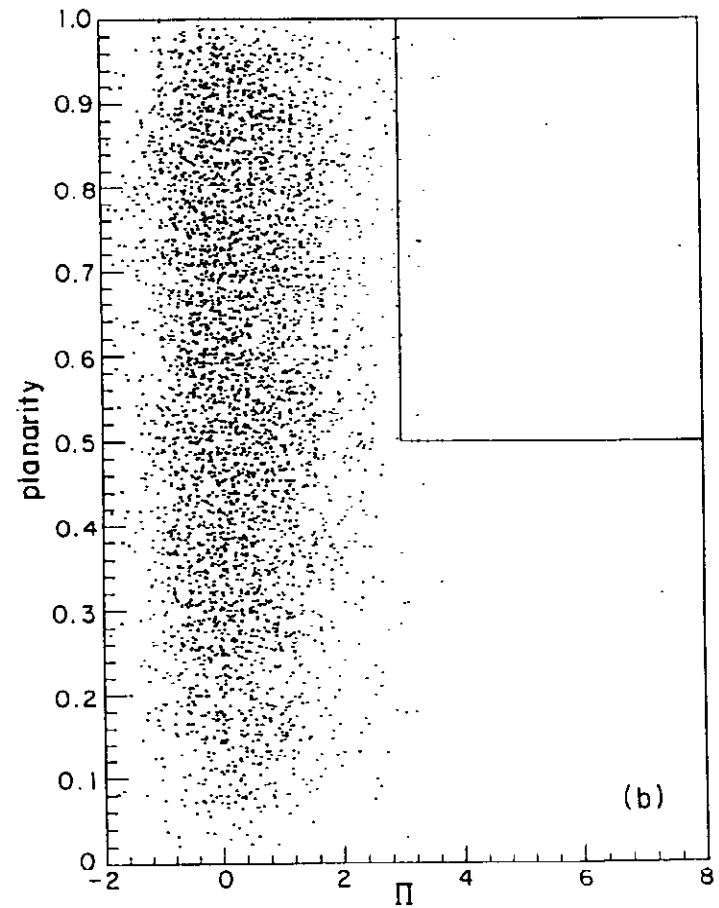
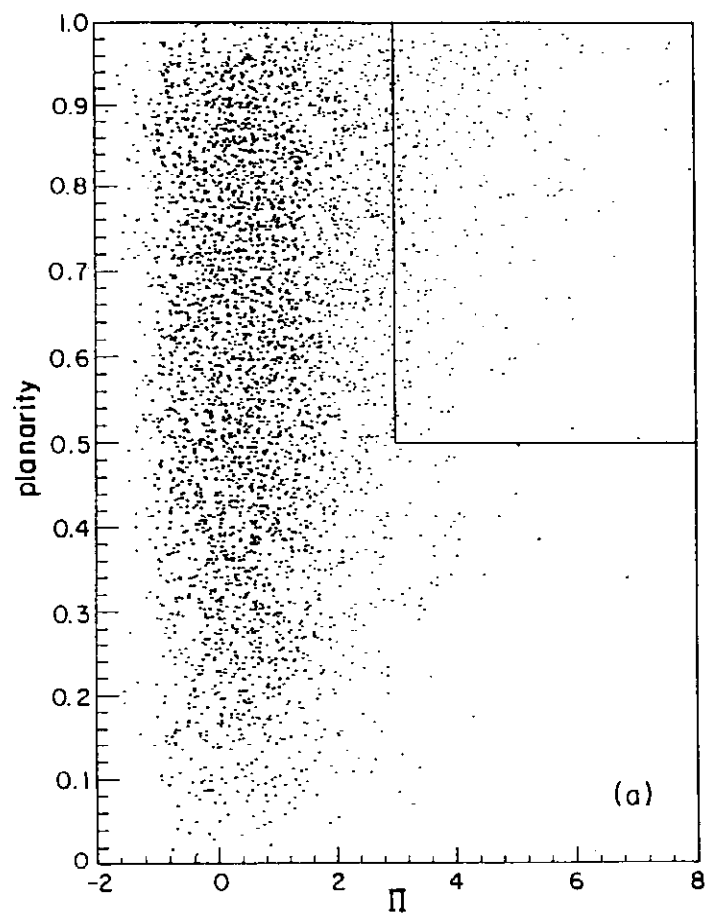


Figure 7: Scatter plots of Π versus \underline{P} for events with $W^2 > 300 \text{ GeV}^2/c^4$ and ≥ 4 charged hadrons, a: Data, b: Monte Carlo without hard QCD. The boxes denote the regions $\Pi > 3.0$ and $\underline{P} > 0.5$.

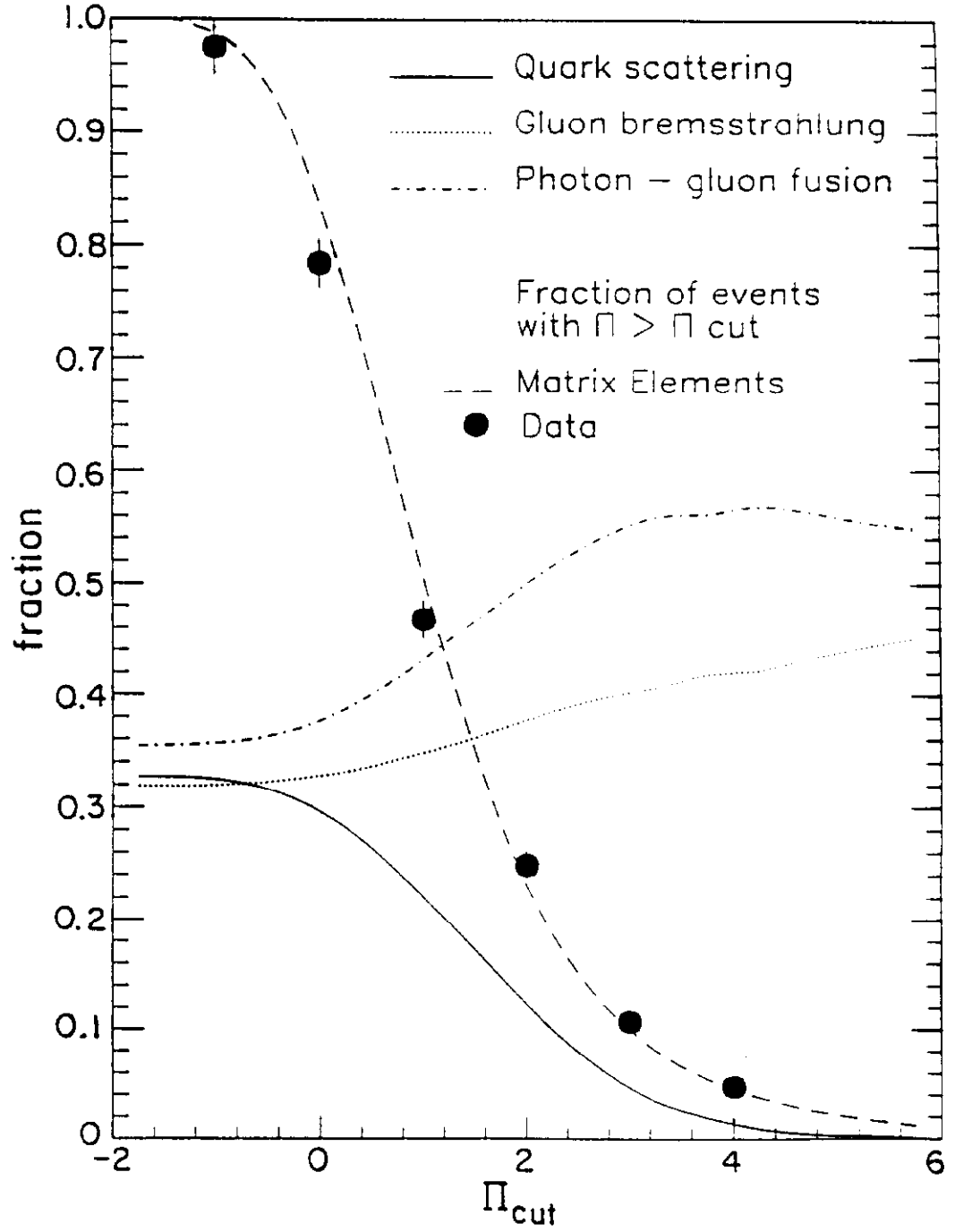


Figure 8: Fraction of Monte Carlo event type for $\Pi > \Pi_{cut}$. Also shown is the fraction of remaining events for $\Pi > \Pi_{cut}$ for data and Monte Carlo. The Lund default value for the gluon-quark threshold, $m_{ij} > 2 \text{ GeV}^2/c^4$, is used. The data are corrected for acceptance.

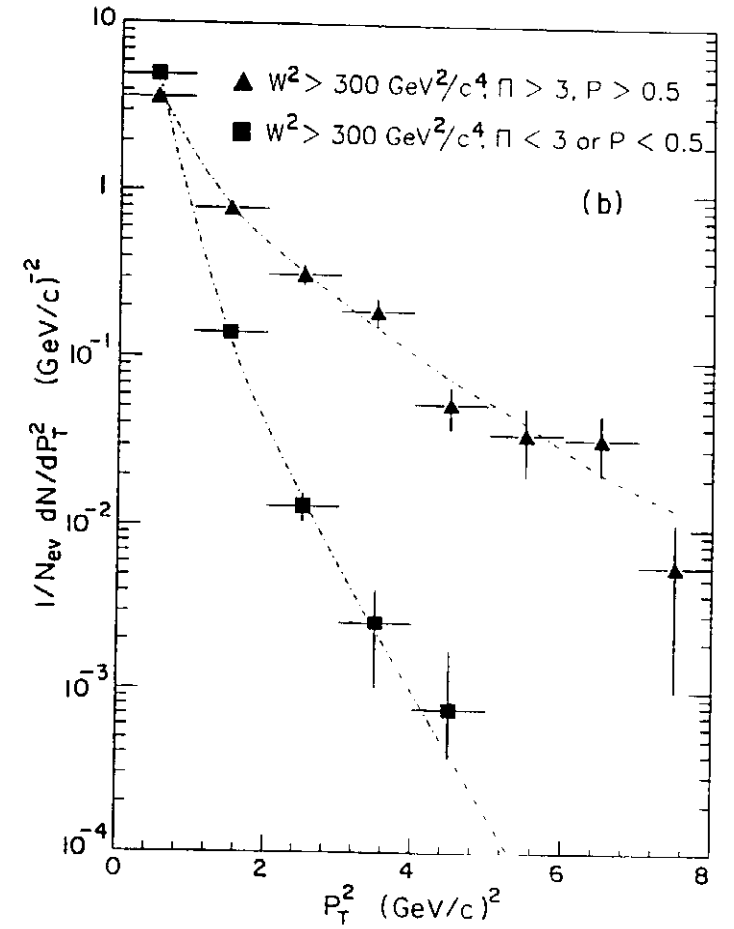
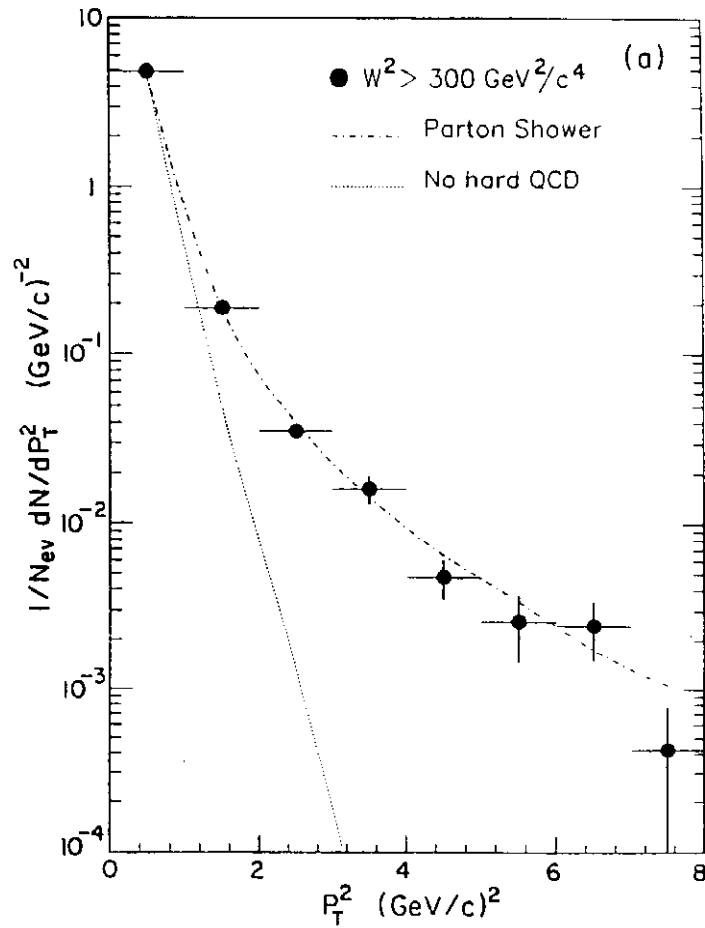


Figure 9: Normalized p_T^2 distributions for events with $W^2 > 300 \text{ GeV}^2/c^4$ and ≥ 4 charged hadrons. In Figure a, all events passing the event cuts are shown. In Figure b, the effect of imposing Π and P cuts is shown. The data are corrected for acceptance.

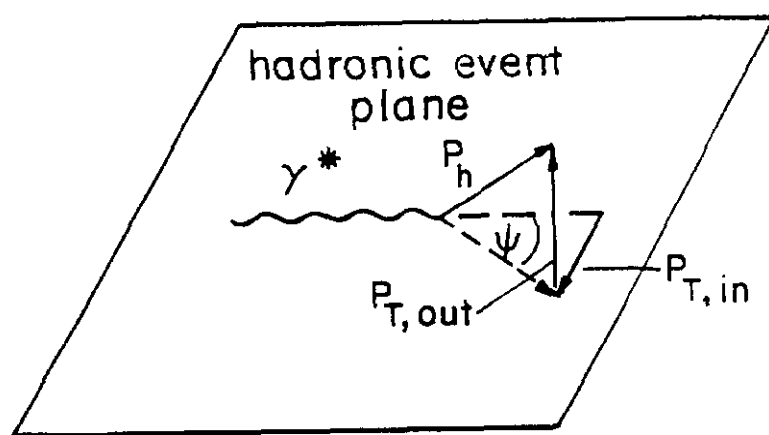


Figure 10: Definition of the angle ψ^j (see text).

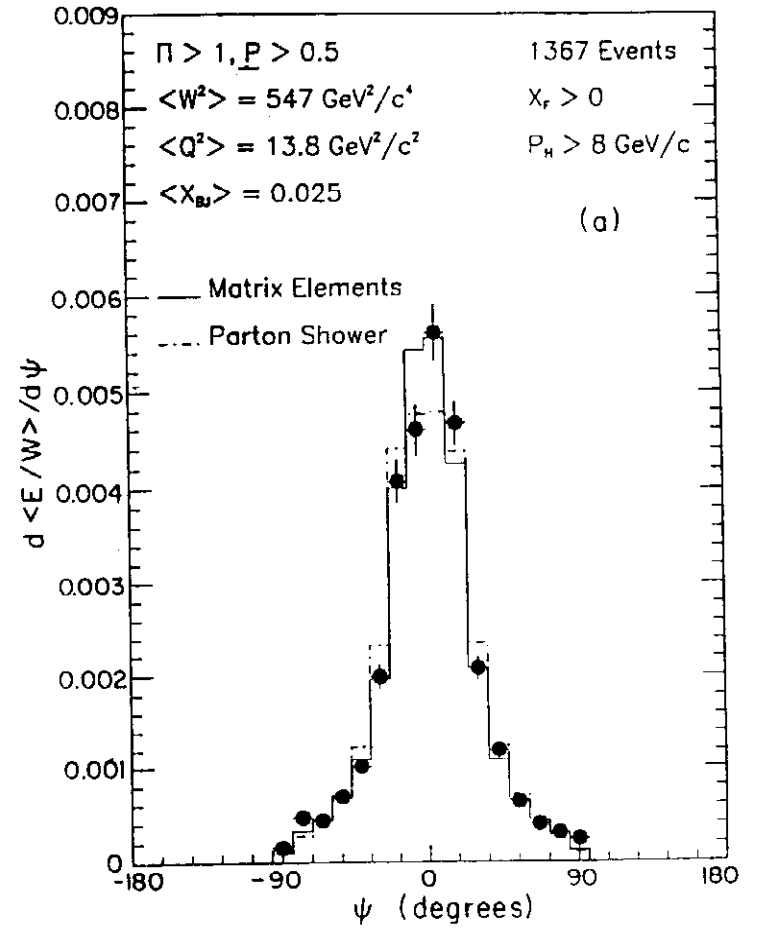
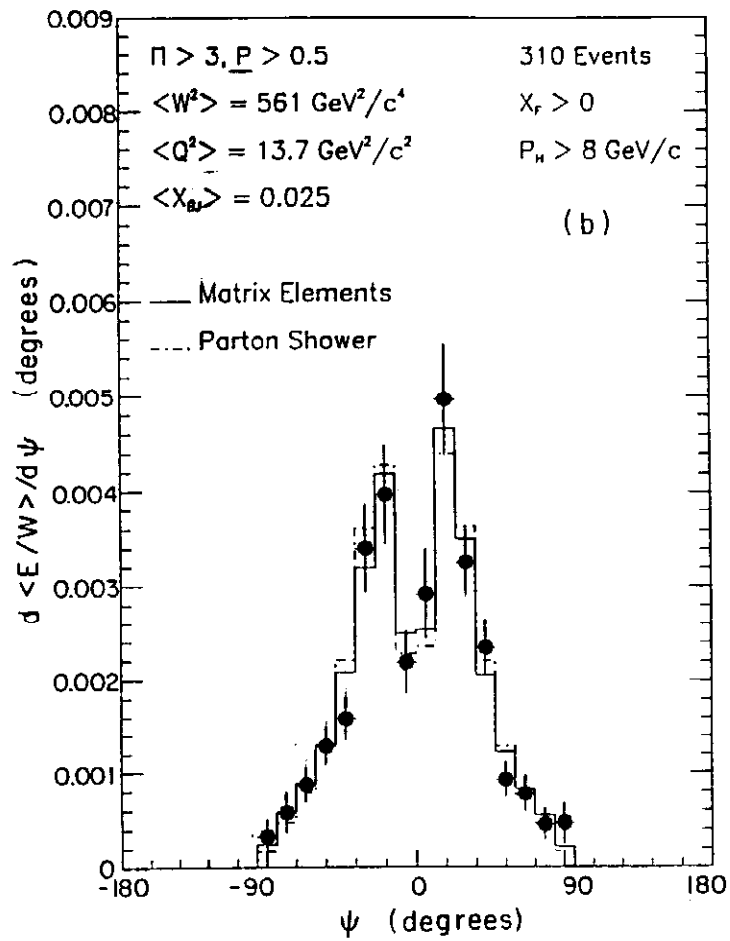


Figure 11: Energy flow profiles for events with $W^2 > 300 \text{ GeV}^2/c^4$, $\underline{P} > 0.5$ and a: $\Pi > 3$, b: $\Pi > -1$. The data are corrected for acceptance. The curves are LUND Matrix Element (solid) and Parton Shower (dot-dashed) Monte Carlo calculations described in the text.

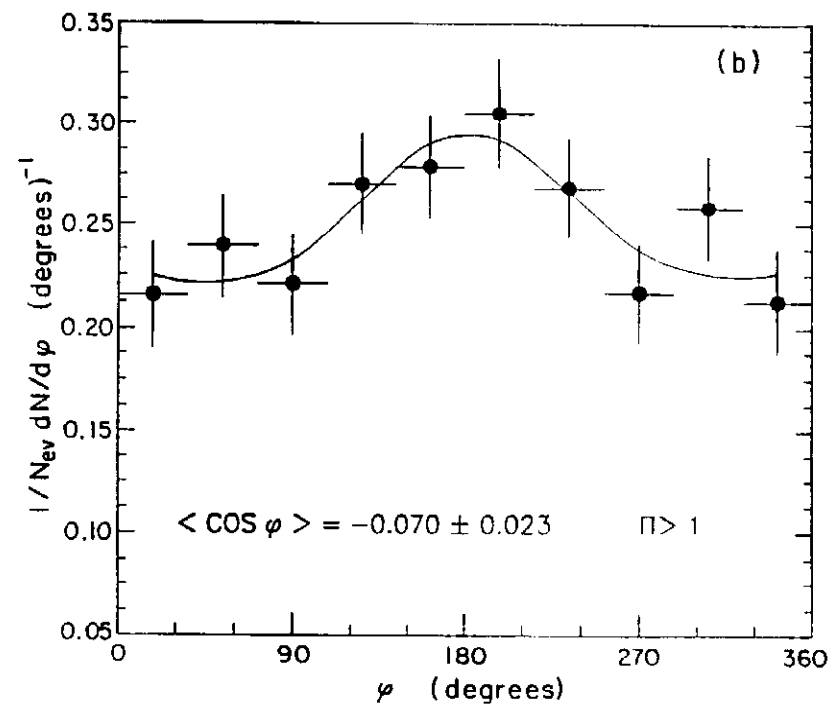
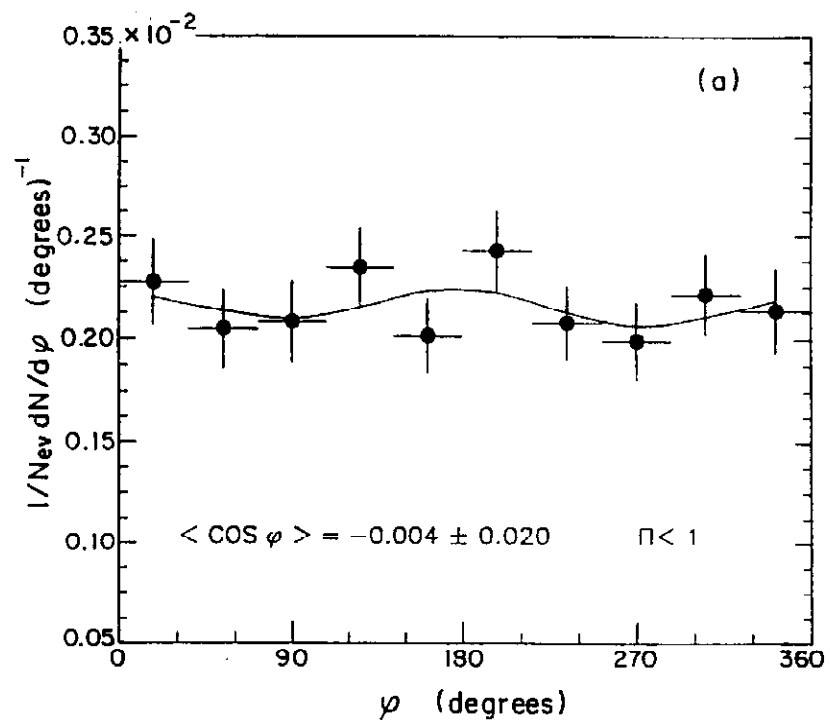


Figure 12: Normalized ϕ distributions for events with a: $\Pi < 1.0$ and b: $\Pi > 1.0$.

The data are corrected for acceptance and the solid lines are fits to the data.

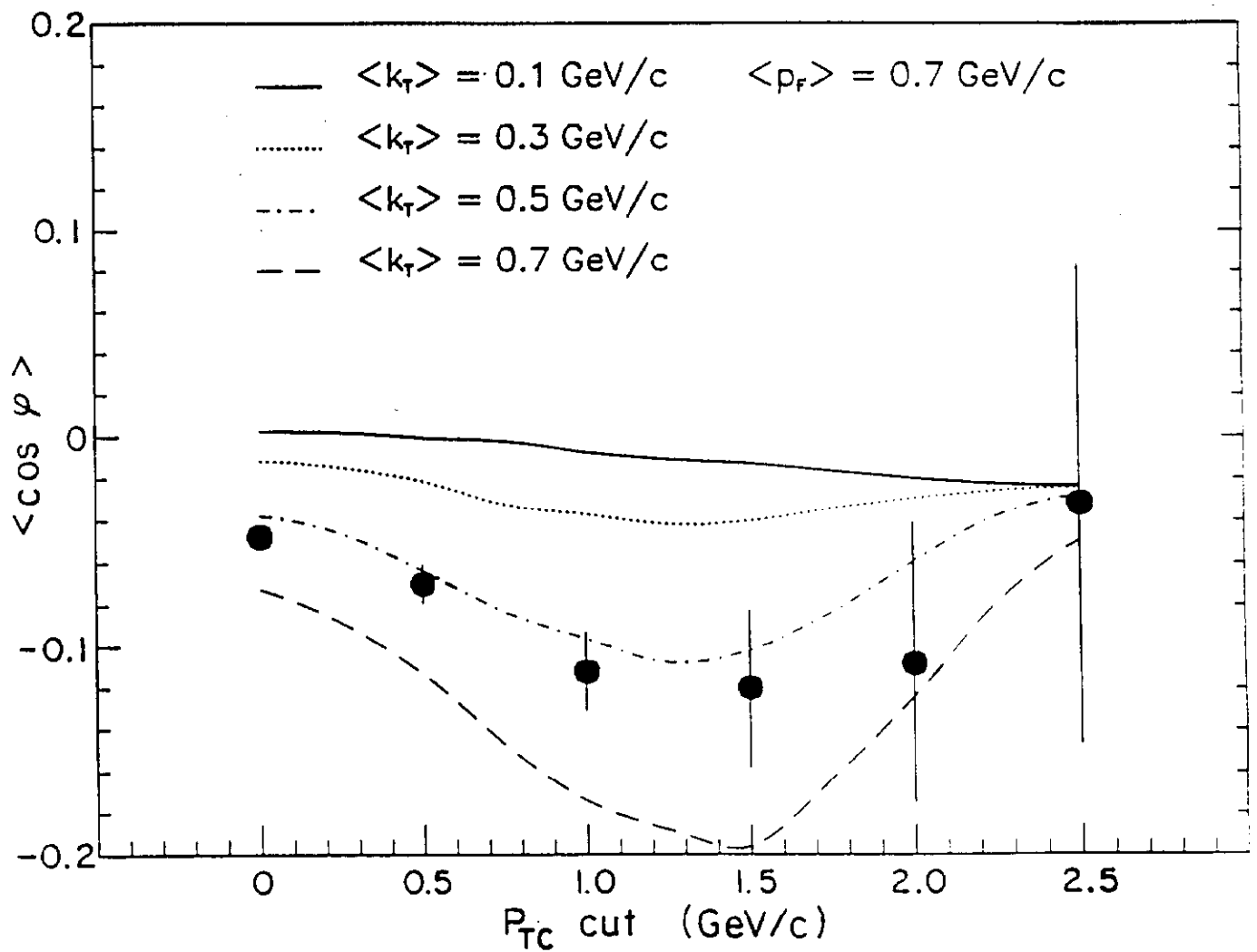


Figure 13: The dependence of $\langle \cos \phi \rangle$ on transverse momentum cutoff. The curves are the predictions of Chay *et al.* [5] for $\langle p_T \rangle = 0.7 \text{ GeV/c}$ and several values of average intrinsic transverse momentum. The data have been corrected for acceptance.